ELSEVIER

Journal of Nuclear Materials 312 (2003) 163–173

journal of nuclear materials

www.elsevier.com/locate/jnucmat

Microstructural evolution in medium copper low alloy steels irradiated in a pressurized water reactor and a material test reactor

K. Fukuya [a,*], K. Ohno [a], H. Nakata [a], S. Dumbill [b], J.M. Hyde [b]

[a] *Institute of Nuclear Safety System Inc., 64 Sata, Mihima-cho, Mikata-gun, Fukui 919-1205, Japan*
[b] *AEA Technology, Nuclear Science, 220 Harwell, Didcot, Oxfordshire OX11 0RA, UK*

Received 17 May 2001; accepted 10 November 2002

Abstract

A533B steels containing 0.12% and 0.16% Cu were irradiated to 3×10^{23} and 6×10^{23} n/m^2 ($E > 1$ MeV) at 290 °C in a pressurized water reactor (PWR) and a material test reactor (MTR). Microstructural changes were examined using atom probe, small angle neutron scattering, field emission gun scanning transmission electron microscopy and post-irradiation annealing (PIA) coupled with positron annihilation (PA) and hardness testing (Hv). Cu rich precipitates had a Cu enriched core with surrounding Ni, Mn and Si rich region and the atomic composition was Fe–(7–16)Cu–(2–8)Mn–(0–4)Ni–(0–4)Si. The size and number density of Cu rich precipitates and the residual Cu concentration in matrix were almost saturated at above 3×10^{23} n/m^2. Low flux irradiation in PWR produced slightly larger precipitates of a lower density with a higher Cu concentration in the precipitates. PIA (PA and Hv) examination showed that vacancy type matrix defects after PWR irradiation were more stable and more effective for hardening than those after MTR irradiation.

PACS: 61.80.Hg; 61.82.Bg; 81.40.Cd; 81.70.Bt

1. Introduction

Radiation hardening and embrittlement of commercial reactor vessel steels is known to be sensitive to various material variables (e.g., Cu content, heat treatment, ...) and irradiation conditions (e.g., flux, temperature, ...). To forecast long life integrity of pressure vessel steels considering various parameters, it is necessary to use predictive models based on physical mechanisms. This requires an understanding of the exact nature of the damage and its evolution during irradiation. The progress in experimental tools such as atom probe (AP), small angle neutron scattering (SANS) and field emission gun scanning transmission electron microscopy (FEGSTEM) enables us to investigate detailed microstructural features in irradiated steels [1,2]. Several types of microstructural features have been proposed and often categorized into two components; precipitates and matrix damage. For Cu rich precipitates which are known to be an important feature causing hardening in high Cu steels, AP and SANS examination showed that the precipitates consist of Fe, Cu, Ni, Mn and Si [3–5]. Mn–Ni–Cu solute clustering [6–8] and Si–Mn precipitates [9] in low Cu steels have also been detected. Matrix damage is recognized as defect clusters or defect-solute complexes [1]. They have not been clearly identified experimentally in pressure vessel steels although the existence of microvoids in irradiated low Cu steels was suggested by SANS experiments [4]. Matrix damage is

* Corresponding author. Tel.: +81-770 37 9114; fax: +81-770 37 2009.
E-mail address: fukuya@inss.co.jp (K. Fukuya).

0022-3115/03/$ - see front matter
doi:10.1016/S0022-3115(02)01675-6

believed to be the dominant feature for hardening in low Cu steels and at high fluences in high Cu steels. Post-irradiation annealing (PIA) coupled with positron annihilation (PA) and hardness testing (Hv) testing is used to investigate the nature of matrix damage in hardening [10–12].

Examination of the microstructures in in-service steels irradiated at different fluxes is especially important to understand embrittlement behavior of industrial materials under plant conditions. In the French pressurized water reactor (PWR) Chooz A, steels with low Cu irradiated to above 1×10^{24} n/m^2 ($E > 1$ MeV) has been extensively studied using AP and SANS [6,7,13–16]. The results indicated clustering of Si, Mn, Ni and Cu and this was discussed in terms of the role of cascade damage for the formation of such clusters. In the in-service steels with medium Cu irradiated to 3×10^{22} n/m^2 in a BWR, Cu–Mn–Ni precipitates and vanadium carbides were detected [3,17]. The archive material was irradiated in material test reactor (MTR) at a higher flux and it was confirmed that lower flux irradiation produced larger and less dense precipitates. Studies on in-service steels are relatively scarce compared to those on alloys irradiated in MTRs under accelerated flux conditions. More experimental evidence is necessary to establish a physical model of microstructural evolution.

The present study is to characterize microstructural evolution in commercial A533B vessel steels with medium Cu content irradiated in a PWR using advanced analytical tools such as AP, SANS, FEGSTEM and PIA (PA/Hv). Together with the results of the same material irradiated in a MTR under high flux condition, the effect of fluence and flux on precipitates and matrix damage is discussed.

2. Experimental

2.1. Materials and irradiation

The steels examined were two heats of A533B class 1 plates; A and B. The chemical compositions are shown in Table 1. The Cu contents were 0.12% and 0.16%. The steel A was austenitized at 880 °C for 4 h, water quenched, then tempered at 660 °C for 6 h and stress relieved at 615 °C for 15.5 h. The steel B was austenitized at 866–871 °C for 7 h, water quenched, then tempered at 649–660 °C for 5.25 h and stress relieved at 610–621 °C for 24.3 h.

The fluence and flux of each sample are shown in Table 2. The A1 sample irradiated to 3.1×10^{23} n/m^2 ($E > 1$ MeV) was taken from a tested surveillance specimen. The time in the reactor was 12 effective full power years. The irradiation temperature was estimated to be 290 °C. The flux and fluence were determined by standard dosimetry methods. The A2, B1 and B2

Table 1
Chemical compositions in wt%

Steel	C	Si	Mn	P	S	Ni	Cr	Mo	Cu	Fe
A	0.12	0.25	1.20	0.014	0.015	0.58	0.08	0.54	0.12	Balance
B	0.17	0.29	1.45	0.011	0.017	0.55	0.11	0.50	0.16	Balance

Table 2
Irradiation conditions

Steel	Sample	Irradiation	Flux n/m^2/s ($E > 1$ MeV)	Fluence n/m^2 ($E > 1$ MeV)
A	A1	PWR	7.8×10^{14}	3.1×10^{23}
	A2	MTR	5.0×10^{16}	6.8×10^{23}
B	B1	MTR	2.3×10^{16}	3.3×10^{23}
	B2	MTR	5.0×10^{16}	5.8×10^{23}

Table 3
Mechanical property data of the irradiated samples

Steel	Sample	Fluence, n/m^2 ($E > 1$ MeV)	Yield stress increase (MPa)	Hardness increase (Hv)	41J transition shift (°C)
A	A1	3.1×10^{23}	93	49	75
	A2	6.8×10^{23}	–	62	85
B	B1	3.3×10^{23}	91	50	79
	B2	5.8×10^{23}	131	86	100

samples were irradiated in the Ford reactor in Chicago University. The temperature was controlled at 290 ± 10 °C. The mechanical property data of the irradiated steels are summarized in Table 3.

2.2. Microstructural examinations

Unirradiated and irradiated samples were examined using AP, SANS, FEGSTEM and PIA (PA/Hv).

AP measurements were carried out using an energy compensating optical position sensitive atom probe facility at Oxford University. The instrument consists of a position-sensitive detector and a high-resolution flight time detector. The mass resolution was approximately 1/600. The samples for AP measurement were cut to make blanks 0.5 mm × 0.5 mm × 20 mm and then electropolished using 25% perchloric in acetic acid to form needle samples. Final polishing was performed using 2% perchloric acid in 2-butoxyethanol. During analysis the sample temperature was kept to below −55 K to prevent any preferential evaporation of Cu.

The SANS measurements were performed at the Institut Laue Langevin, Grenoble, using the 35 m SANS instrument, D11, installed on the ILL High Flux Reactor. Measurements on samples 10 mm × 10 mm × 2 mm were made in zero magnetic field and in a magnetic field of $\geqslant 1.0$ T both parallel and perpendicular to the wavevector. A mean wavelength of 0.45 nm was used. The neutron scattering cross-section data was analyzed using a maximum entropy method to extract the most probable precipitate size distributions, assuming spherical particles. The absolute volume fraction of precipitate and number density were determined based on the A ratio (the ratio of the irradiation-induced scattering intensities in directions perpendicular and parallel to the applied magnetic field) from SANS measurement and precipitate chemical composition from AP measurement.

TEM observations were performed using a Phillips EM430 operating at 300 kV. The precipitate compositions were measured using VG HB501 FEGSTEM operating at 100 kV. The probe beam diameter for spot measurement was typically 2 nm. The samples were prepared by electropolishing in 5% perchloric in acetic acid at −45 °C.

The PIA (PA/Hv) experiments were performed using positron annihilation lineshape analysis (PALA) and hardness measurements after isochronal annealing at temperatures ranging from 250 to 450 °C at 50°C interval for 0.5 h. PALA is a Doppler broadening technique, in which the change in the energy profile of 511 keV γ rays was measured and quantified as the S parameter. In this study the change was measured by ΔS, defined as the difference between an irradiated sample and an unirradiated reference sample made of the same material. Vickers hardness measurement was carried out using a 20 kgf load.

3. Results

3.1. Precipitates

Cu rich precipitates in the irradiated materials were detected by high resolution TEM observation under a high-angle annular dark-field condition and FEGSTEM/EDS analysis as shown in Fig. 1. The precipitates contained Cu, Ni, Mn and P. No evidence of such Cu rich precipitates was detected in the unirradiated samples. TEM observations revealed that pre-existing dislocations and carbides such as Mo_2C were not changed due to irradiation.

The detailed structure and composition of the precipitates were obtained using AP measurements. Fig. 2 shows a series of three-dimensional atom maps of the solutes in steel A irradiated in a PWR to 3.1×10^{23} n/m^2

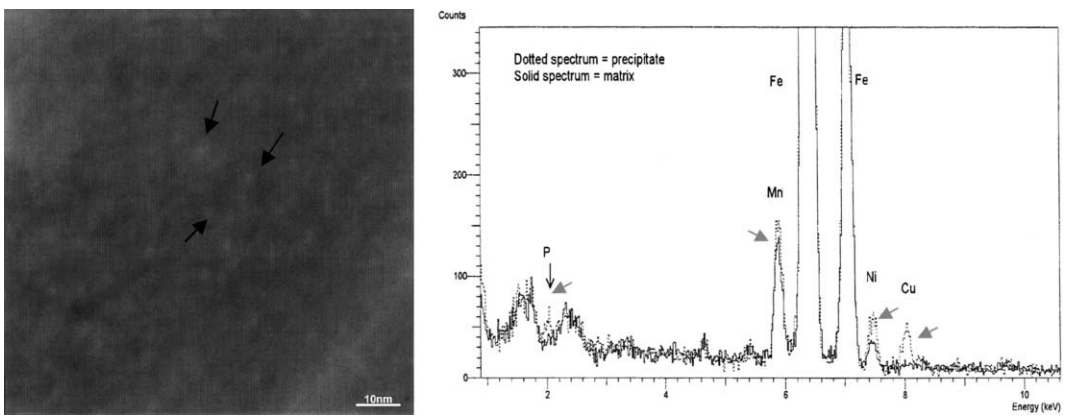

Fig. 1. Dark field image and EDX spectrum from Cu rich precipitates in steel A irradiated in a PWR to 3×10^{23} n/m^2 ($E > 1$ MeV).

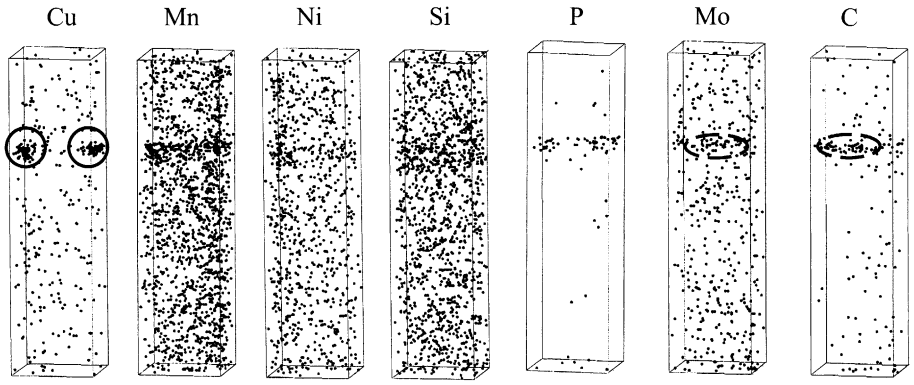

Fig. 2. 3D atom map of the solutes in 10 nm × 10 nm × 40 nm region in steel A irradiated in a PWR to 3×10^{23} n/m^2 ($E > 1$ MeV).

(A1). Two Cu rich precipitates were detected near a region enriched in Mo and C, presumably Mo_2C carbide. Both carbide and precipitates in Fig. 2 located in the matrix. Fig. 3 shows atom maps in steel B irradiated in MTR to 5.8×10^{23} n/m^2 (B1), showing three Cu rich precipitates. The Cu rich precipitates containing Ni, Mn and Si were detected in the matrix in all the irradiated samples. The diameter was typically around 2 nm. All the precipitates detected consisted of a centered region enriched in Cu atoms and a surrounding region enriched in Ni, Mn and Si atoms. These solute distributions in the precipitates were confirmed in enlarged views of AP atom maps as shown in Fig. 4. Table 4 shows the average composition of the precipitates by calculating the solute fraction in the center 1.5 nm × 1.5 nm × 1.5 nm region of the precipitates. The range of precipitate compositions was Fe–(7–16)Cu–(2–8)Mn–(0–4)Ni–(0–4)Si. It was confirmed by AP analysis that P atoms were not contained in the precipitates although P was often detected in 2 nm spot analysis using FEGSTEM. The Cu and Mn contents in the precipitates were slightly higher for the PWR-irradiated sample. The difference in composition between the three MTR-irradiated samples was very small.

Fig. 5 shows results of SANS measurements on each sample without magnetic field, the differential neutron scattering cross section I vs. scattering vector Q^2. The A1 curve was different from curves of A2, B1 and B2, indicating that the size distribution of scattering centers in A1 sample differs from the others. The volume fraction vs. diameter derived from these data using a maximum entropy method assuming the scattering centers are spherical are shown in Fig. 6. SANS analyses indicated the presence of scattering centers with an average diameter of about 2 nm. This value is very consistent with the precipitate diameter from TEM and AP observations. The range of size distribution was from 1.5 to 5.5 nm for all materials. No difference in the range was observed while the peak position of A1 material was higher than those of the other material. The average diameter in the surveillance material A1, 2.6 nm, was slightly higher than those in the other samples irradiated in MTR at a higher flux. The estimated number density is shown in Table 5 with data of the A ratio and volume fraction. The volume fraction and number density in B2 are slightly higher than those in A2, suggesting that the nucleation of Cu rich precipitate is dependent on the initial Cu content. The diameter and number density in

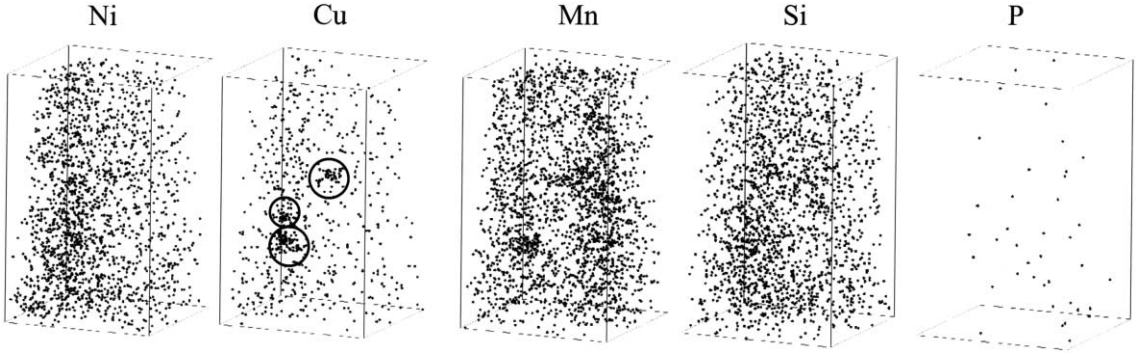

Fig. 3. 3D atom map of the solutes in 18 nm × 18 nm × 30 nm region in steel B irradiated in a MTR to 3×10^{23} n/m^2 ($E > 1$ MeV).

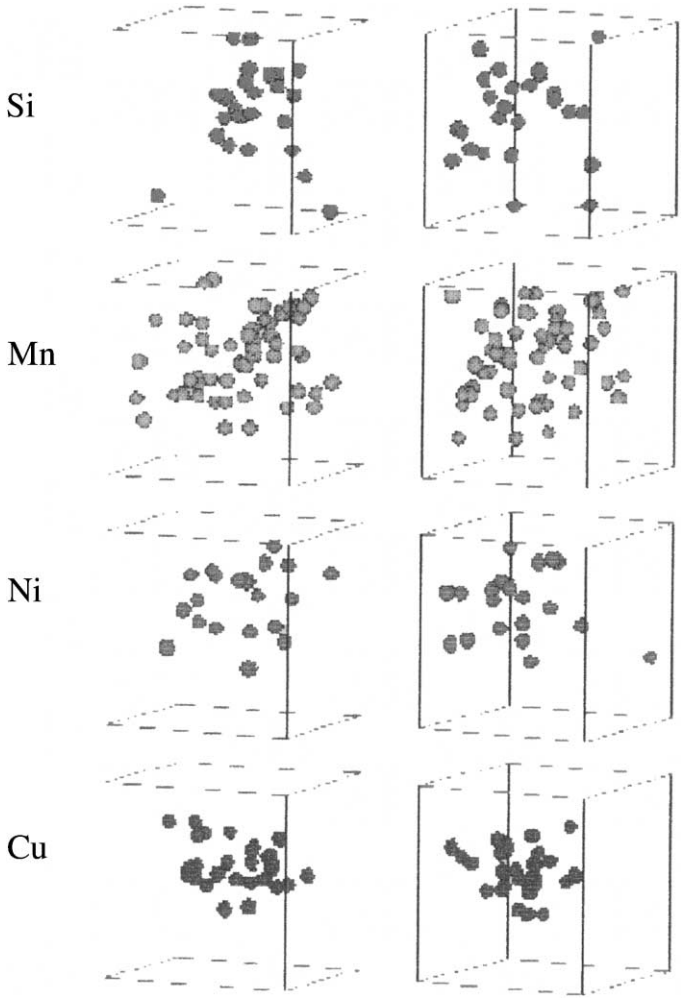

Fig. 4. Pairs of 3D maps from orthogonal angles showing Si, Mn, Ni and Cu distribution in a Cu rich region (4 nm × 4 nm × 4 nm) in A irradiated in a MTR to 6×10^{23} n/m^2 ($E > 1$ MeV).

Table 4
Average composition of precipitates

Steel	Sample	Fluence n/m^2 ($E > 1$ MeV)	Composition (at.%)
A	A1	3.1×10^{23}	63Fe–15Cu–8Mn–7Ni–4Si
	A2	6.8×10^{23}	80Fe–11Cu–4Mn–4Ni–1Si
B	B1	3.3×10^{23}	74Fe–11Cu–4Mn–7Ni–2Si
	B2	5.8×10^{23}	78Fe–9Cu–5Mn–6Ni–3Si

steel B showed a small change at fluences ranging from 3.3×10^{23} to 5.8×10^{23} n/m^2. At these fluences, nucleation and growth of Cu rich precipitates were considered to be saturated. The number density in sample A1 is much smaller than the expected value from A2 considering the difference in B1 and B2.

Precipitation or solute enrichment other than Cu rich precipitates was found. Fig. 7 shows an example of an AP atom map of P viewed from two different directions. These P enriched regions were detected only in the higher fluence samples A2 and B2. These can be assumed to be needle-like Fe-phosphide or P segregation

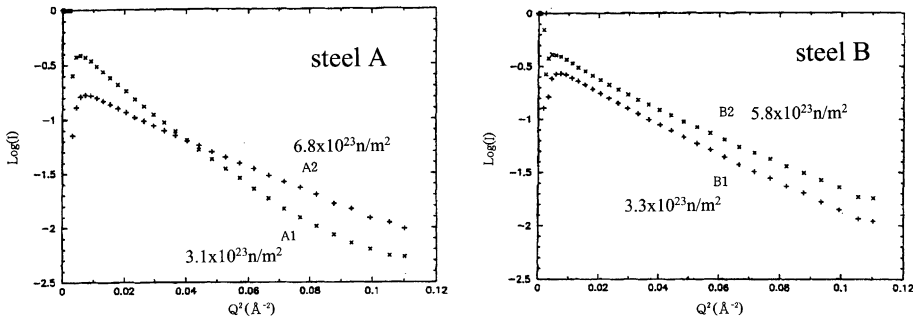

Fig. 5. Plots of $\log(I)$ vs. $Q2$ where I is the normalized background corrected, radially averaged data for differential (irradiated sample cross section–unirradiated sample cross section) in zero magnetic field.

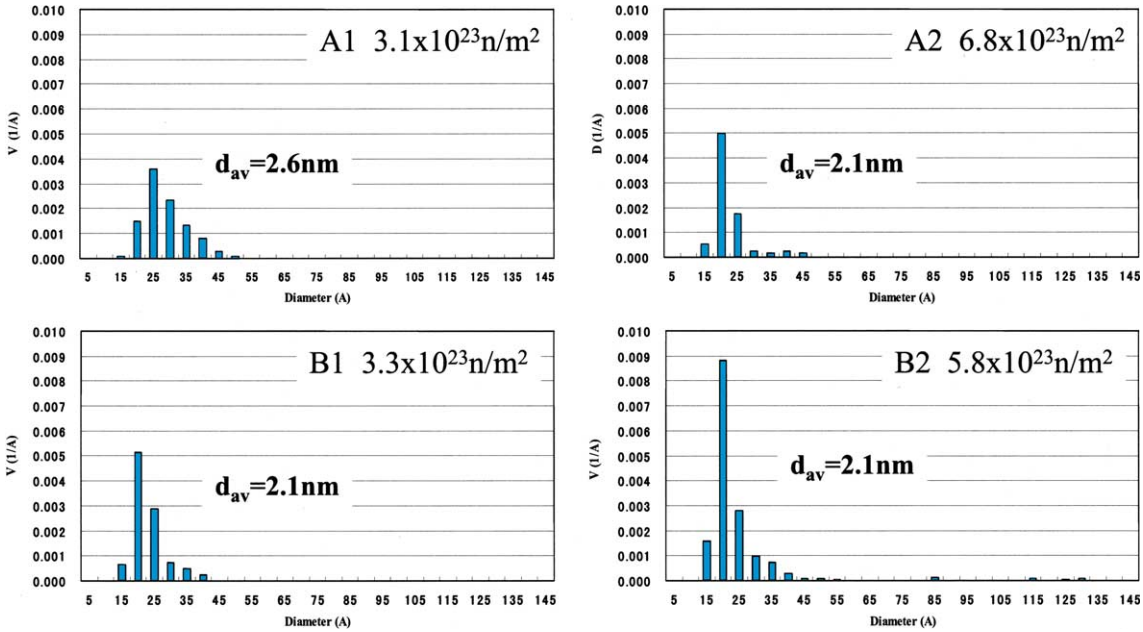

Fig. 6. Volume weighted particle size distributions of precipitates determined by SANS.

Table 5
Summary of precipitates data determined by SANS

Steel	Sample	Fluence, n/m^2 ($E > 1$ MeV)	Average diameter (nm)	A ratio	Volume fraction	Number density (m^{-3})
A	A1	3.1×10^{23}	2.6	2.87	0.0038	4.1×10^{23}
	A2	6.8×10^{23}	2.1	3.07	0.0046	9.5×10^{23}
B	B1	3.3×10^{23}	2.1	3.06	0.0053	1.1×10^{24}
	B2	5.8×10^{23}	2.1	2.71	0.0064	1.3×10^{24}

on a dislocation. Analyses of elements distribution near this feature confirmed some enrichment of Cu, Mn and Si around the feature. No enrichment of other elements such as C was detected near this feature. The detailed nature of these features and whether these are radiation-induced or not, was difficult to be determined because the AP only enables the analysis of a very small volume.

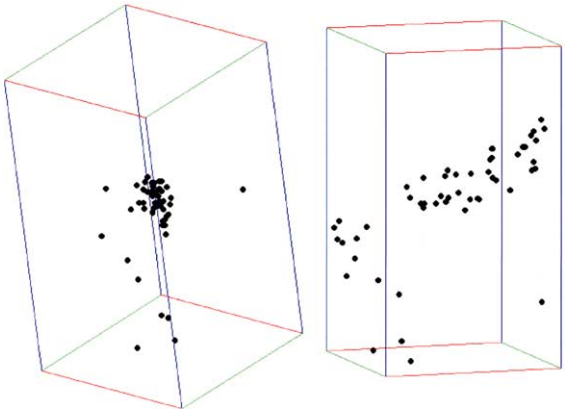

Fig. 7. Two orthogonal views showing one-dimensional P atom distribution in steel B irradiated in a MTR to 6×10^{23} n/m^2 ($E > 1$ MeV).

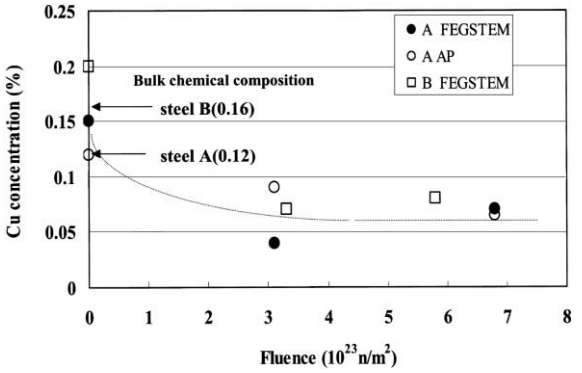

Fig. 8. Cu concentration in matrix as a function of fluence.

3.2. Matrix Cu concentration

The matrix Cu concentration determined using FEGSTEM and AP as a function of fluence is shown in Fig. 8. In the case of FEGSTEM the value was determined by averaging the lower five data values among 20 spot measurements. The AP value was determined by subtracting the Cu contained in the clusters from that measured in the whole analyzed volume. The measured Cu concentration in matrix was decreased to around 0.07% at 3×10^{23} n/m^2 and saturated for further irradiation. The calculated residual Cu concentration in the matrix using the measured volume fraction and composition data of Cu precipitates was around 0.1%, which is consistent with the measured matrix value. The saturation of residual Cu concentration in the matrix is consistent with the result that the evolution of Cu rich precipitates (size, number density and composition) is almost saturated at above 3×10^{23} n/m^2 as shown by the AP and SANS measurements.

3.3. Matrix damage

Neither TEM nor FEGSTEM observations could detect any evidence for the formation of microvoids and dislocation loops, which are the assumed form of the matrix damage. PIA experiments combining PALA and Hv measurements are known to be sensitive to the stability of vacancy type defects and/or precipitates in irradiated steels. Fig. 9 shows the recovery behavior of the S-parameter and hardness in A1 and A2. The A2 sample showed higher ΔS than A1 sample in the as-irradiated condition. This indicates that A2 contained a higher concentration of vacancy-type defects as expected because the fluence in A2 was twice of that in A1. No recovery was observed in either sample at temperatures below 300 °C. At 350 °C A2 showed an indication of recovery in ΔS but this was not clear. Both samples showed rapid recovery of ΔS ($\approx$0) at 400 °C and further recovery to below zero at 450 °C. The ΔS recovery at 400 °C was much higher for the A1 sample while Hv recovery was nearly identical in both samples. The negative ΔS value suggests some change of Cu rich precipitation in conjunction with matrix damage annealing. The difference in the degree of recovery at 400°C between A1 and A2 samples is considered to reflect the thermal stability of matrix damage and possibly the Cu rich precipitates.

4. Discussions

4.1. Cu precipitation

The present study showed the detailed structure and composition of Cu rich precipitates in medium Cu steels irradiated in a commercial PWR and a MTR. It was confirmed that the higher flux MTR irradiation produces precipitates with smaller size, higher density and lower Cu content. In order to compare our data with published works, data on the diameter and number density of precipitates and/or cluster are summarized in Fig. 10 as a function of fluence. The data in this figure were selected for A533B steels which have similar Cu, Ni and P contents to those in the present study. The difference in flux between in-service data and MTR data in Fig. 10 was in the order of 10^2. The diameter of precipitates in in-service irradiated steels ranged from 2 to 4 nm, and was larger than in MTR irradiated steels (typically $<$2 nm). The precipitate number density in MTR irradiated steels is higher than in in-service irradiated steels.

Regarding the structure and composition of the precipitates, the reported information measured by the advanced AP technique is quite poor except for French PWR data on low Cu steel (0.09 wt% Cu). In that study the cluster composition in atomic fraction was found to

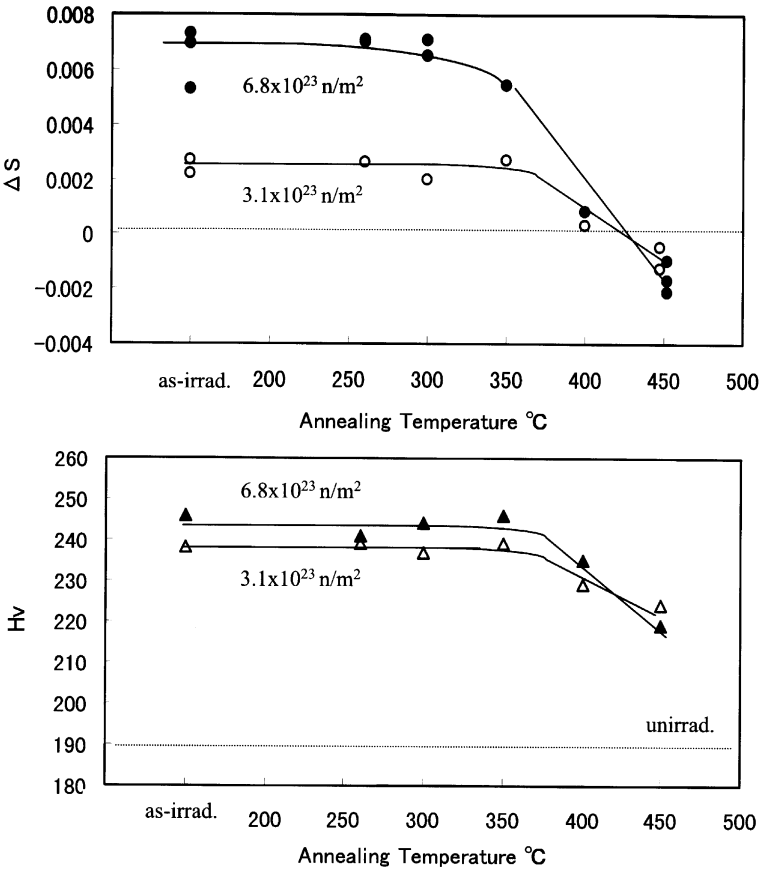

Fig. 9. Recovery of ΔS and hardness in steel A during annealing for 0.5 h.

be Fe–(1.0–2.7)Si–(1.3–4.7)Ni–(1.6–7.4)Mn–(0.5–0.9)Cu at 2.5×10^{23} n/m^2 and the solutes were uniformly distributed in the clusters. In the present study the precipitate composition was Fe–(0–4)Si–(0–4)Ni–(2–8)Mn–(7–16)Cu and there existed a Cu rich core in the precipitates. While the Cu content in the precipitates in our sample was one order of magnitude higher than that in the French data, the concentrations of Si, Ni and Mn are quite comparable level in both sets of data. Furthermore, in the present study the structure and composition of the precipitates were nearly identical among the samples analyzed in spite of the difference in the initial Cu content, fluence and flux. The above data seem to imply that the enrichment of Mn, Ni and Si is independent of the existence of Cu. The mechanism of precipitate formation in low alloy steels during irradiation has been considered to be through the aggregation of supersaturated Cu atoms due to radiation-enhanced diffusion [1]. Under the framework of this model, it is possible to explain our observations so that Cu aggregation occurs first and then Ni, Mn and Si segregate during further irradiation or that simultaneous clustering of Cu, Ni, Mn and Si occurs followed by redistribution of the solutes in the clustered region. An alternative mechanism for clustering of the solutes is that damaged regions associated with the displacement cascades act as nucleation sites in the low Cu steel (<0.1%) [7,16]. It is not clear if this model can be applied to the structure of precipitates observed in this study, where there is a Cu rich core and surrounding Ni, Mn and Si region. However, the fact that the size and number density of precipitates and that the Ni, Si and Mn contents in the precipitates at around 3×10^{23} n/m^2 was quite similar between our A2 sample (0.12%Cu) and Chooz A steel (0.09%Cu) may imply some common enrichment mechanism of Ni, Mn and Si during low flux irradiation.

4.2. Matrix damage

PIA studies on irradiated steels containing Cu can give us only indirect information on the matrix damage component because both the line shape parameter and hardness are sensitive to the change in size and composition of the Cu rich precipitates during annealing. However, results from the previous studies using PIA

●	This study	PWR	Cu=0.12	SANS+AP
○	Van Duysen et al.[13]	PWR(Chooz A)	0.09	SANS
□	Auger et al.[6,7,14]	PWR(Chooz A)	0.09	AP
△	English et al.[3]	BWR(KRB-A)	0.16	SANS+FEGSTEM
◇	Kampmann et al.[22]	Low flux	0.2	SANS
■	This study	FNR	0.12, 0.16	SANS+AP
×	Buswell et al.[4]	PLUTO	0.14, 0.16	SANS+FEGSTEM
+	Solt et al.[8]	SAPHIR	0.16	SANS

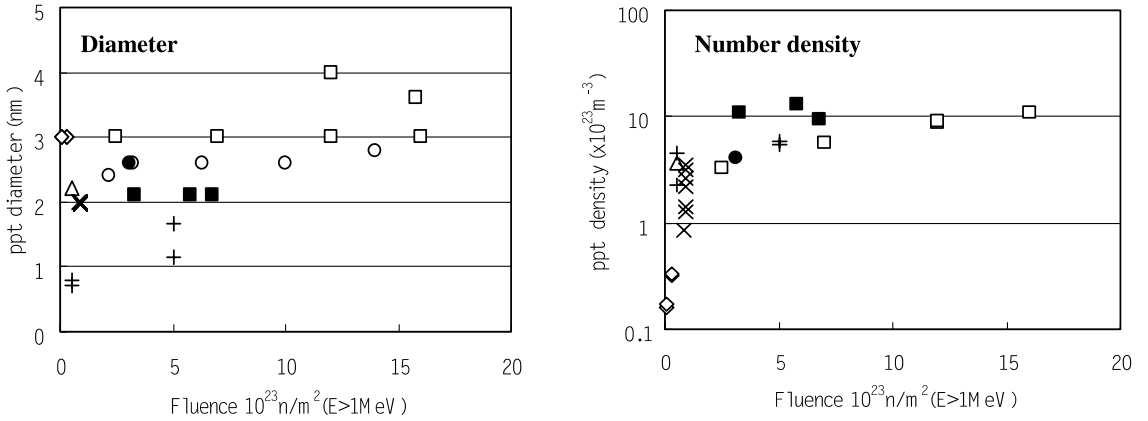

Fig. 10. Fluence dependence of diameter and number density of Cu rich precipitate in in-service irradiated steels and in MTR irradiated commercial alloys containing Cu, Ni and P similar to those of this study.

coupled with PA [10,11,15,18,19] have some bearing on the present results. The general trend is very similar to that observed by Carter et al. [10] for high Cu welds where recovery was observed at 350 °C and a negative ΔS was observed following the anneal at 450 °C. In the as-irradiated condition, the measured ΔS was significantly greater for the MTR irradiated samples. This is consistent with the higher fluence in the sample, which contains more Cu rich precipitates and presumably more matrix damage. The larger recovery in ΔS at 400 °C for MTR irradiation suggests that the higher flux MTR irradiation decreased the thermal stability of vacancy type matrix damage. This is consistent with the previous observations in a low Cu steel [10,19]. Furthermore, similar hardness recovery at 400 °C suggests that defects produced at a higher flux are less effective in producing hardening.

4.3. Correlation with yield stress increase

Based on the quantitative data on Cu rich precipitates, their hardening contribution can be calculated using the Russell Brown dispersion hardening model [20]. Assuming that interaction between line dislocations and precipitates is a function of the modulus difference between matrix and precipitates, the yield stress increase, $\Delta\sigma_{\mathrm{ppt}}$, is given by the following equations:

$$\Delta\sigma_{\mathrm{ppt}} = F_{\mathrm{s}}\tau,$$

$$\tau = Gb/L\left\{1 - (E_1/E_2)^2\right\}^{3/4},$$

$$E_1/E_2 = G_1/G_2\log(r/r_0)/\log(R/r_0) + \log(R/r)/\log(R/r_0),$$

where F_{s} is the Schmidt factor (= 2.5), τ is the shear stress, b is the Burgers vector (= 2.5 nm), L is the precipitate spacing, G is the matrix shear modulus (= 49 GPa), G_1/G_2 is the ratio of precipitate shear modulus to matrix shear stress, r is the precipitate radius, r_0 is the inner cut-off radius of dislocations (= 2.5 b), R is the outer cut-off radius of dislocation (= $1000r_0$). G_1/G_2 is dependent on precipitate composition and structure but is not known for the measured composition in this study. For pure Cu precipitates a value 0.6 has been used [20]. The total yield stress increase can be determined according to $\Delta\sigma_y = (\Delta\sigma_{\mathrm{ppt}}^2 + \Delta\sigma_{\mathrm{md}}^2)^{1/2}$ where $\Delta\sigma_{\mathrm{md}}$ is the contribution of matrix damage. Unfortunately no quantitative information regarding the matrix damage component was obtained in this study. The present PIA results showed that after 400 °C annealing ΔS fell to nearly zero and that ΔHv recovered to about 70% of the as-irradiated ΔHv. Although the recovery is attributed to both matrix damage recovery and change in Cu rich precipitates, if we assume that only the matrix damage is recovered at 400 °C, the contribution of matrix damage to hardening could be estimated to be below 30%. Fig. 11 shows a comparison of the measured yield stress

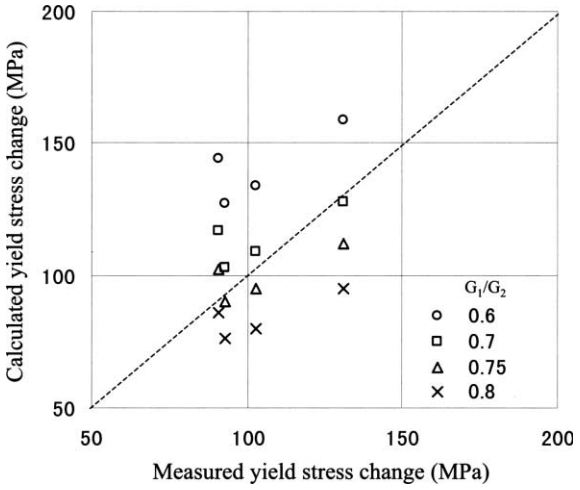

Fig. 11. Comparison of the measured yield stress changes with those calculated by Russell Brawn model changing the ratio of shear modulus in precipitate (G_1) and matrix (G_2).

increase with the calculated increase $\Delta\sigma_{ppt}$ changing G_1/G_2 from 0.6 to 0.8. A good agreement is found when G_1/G_2 is around 0.75 taking into account some contribution of matrix damage. Kampmann et al. [21] reported that the $\Delta\sigma_{ppt}$ estimation using $G_1/G_2 = 0.6$ resulted in good agreement with the measured value in as-irradiated high Cu materials (0.2–0.4%Cu). Thus it appeared that the precipitates examined in this study are elastically harder than those detected by Kampmann et al. [21]. This difference may be due to Cu content in the precipitates based on the observation that this increases with the initial bulk Cu concentration [1].

5. Conclusions

Detailed examination of microstructural changes in commercial A533B steels containing medium Cu levels and irradiated in PWR and MTR shows that Cu rich precipitates have Cu enriched cores with surrounding Ni, Mn and Si rich regions. The size and number density of Cu rich precipitates and the residual Cu concentration in the matrix was almost saturated at 3×10^{23} n/m^2 ($E > 1$ MeV). High flux MTR irradiation produced smaller and more dense precipitates with higher Cu content than in-service PWR irradiation. PIA experiments suggest that matrix damage under MTR irradiation is more thermally unstable and less effective for hardening.

Acknowledgement

The authors wish to thank The Kansai Electric Power Company, Inc. for providing samples and supporting this study.

References

[1] G.R. Odette, G.E. Lucas, Radiat. Eff. Defects Solids 144 (1998) 189.
[2] W.J. Phythian, C.A. English, J. Nucl. Mater. 205 (1993) 162.
[3] C.A. English, W.J. Phythian, J.T. Buswell, J.R. Hawthorne, P.H.N. Ray, in: Proceedings of 15th International Symposium on Effects of radiation on Materials, ASTM STP 1125, ASTM, 1992, p. 93.
[4] J.T. Buswell, W.J. Phythian, R.J. McElroy, S. Dumbill, P.H.N. Ray, J. Maceand, R.N. Sinclair, J. Nucl. Mater. 225 (1995) 196.
[5] M.K. Miller, M.G. Burke, J. Nucl. Mater. 195 (1992) 68.
[6] P. Auger, P. Pareige, M. Akamatsu, J.-C. Van Duysen, J. Nucl. Mater. 211 (1994) 194.
[7] P. Auger, P. Pareige, S. Welzal, J.-C. Van Duysen, J. Nucl. Mater. 280 (2000) 331.
[8] G. Solt, F. Frisius, W.B. Waeber, P. Tipping, in: Proceedings of 16th International Symposium on Effects of Radiation on Materials, ASTM STP 1175, ASTM, 1993, p. 444.
[9] M.K. Miller, K.F. Russel, J. Kocik, E. Keilova, J. Nucl. Mater. 282 (2000) 83.
[10] R.G. Carter, T. Onchi, N. Soneda, K. Dohi, J.M. Hyde, C.A. English, M.T. Hutching, W. Server, J.F. Coste, J.-C. Van Duysen, in: Proceedings of Fontevraud IV, Contribution of Materials Investigation to the problems encountered in pressurized water reactor, September 1998, p. 89.
[11] W.J. Phythian, N. de Diego, J. Mace, R.J. McElroy, in: Proceedings of 16th International Symposium on Effects of Radiation on Materials, ASTM STP 1175, ASTM, 1993, p. 462.
[12] A. Hampel, M. Saneyasu, Z. Tang, M. Hasegawa, G. Brauer, F. Plazaola, S. Yamaguchi, F. Kano, A. Kawai, in: Proceedings of 19th International Symposium on Effects of Radiation on Materials, ASTM STP 1366, ASTM, 2000, p. 560.
[13] J.-C. Van Duysen, J. Bourgoin, C. Janot, J.M. Penisson, in: Proceedings of 15th International Symposium on Effects of radiation on Materials, ASTM STP 1125, ASTM, 1992, p. 117.
[14] P. Auger, P. Pareige, M. Akamatsu, D. Blavette, J. Nucl. Mater. 225 (1995) 225.
[15] P. Pareige, P. Auger, S. Welzel, J.-C. Van Duysen, S. Miloudi, in: Proceedings of 19th International Symposium on Effects of Radiation on Materials, ASTM STP 1366, ASTM, 2000, p. 435.
[16] S. Miloudi, J.C. Van Duysen, P. Auger, P. Pareige, in: Proceedings of 7th International Symposium on Environmental Degradation on Materials in Nuclear Power Systems-Water Reactors, NACE, 1995, p. 1179.
[17] M.G. Burke, S.P. Grant, M.K. Miller, in: Proceedings of 4th International Symposium on Environmental Degradation on Materials in Nuclear Power Systems-Water Reactors, NACE, 1989, p. 2.
[18] M. Valo, R. Krause, K. Saarinen, P. Hautojarvi, J.R. Hawthorn, in: Proceedings of 15th International Symposium on Effects of Radiation on Materials, ASTM STP 1125, ASTM, 1992, p. 172.

[19] G.R. Odette, E.V. Mader, G.E. Lucas, W.SJ. Phythian, C.A. English, in: Proceedings of 16th International Symposium on Effects of Radiation on Materials, ASTM STP 1175, ASTM, 1993, p.373.
[20] K.C. Russel, L.M. Brown, Acta Metall. 20 (1972) 969.
[21] R. Kampmann, F. Frisius, H. Hackbarth, P.A. Beaven, R.Wagner, J.R. Hawthorne, in: Proceedings of 7th International Symposium on Environmental Degradation on Materials in Nuclear Power Systems-Water Reactors, NACE, 1993, p. 679.